Compound droughts slow down the greening of the Earth

Xianfeng Liu, Gaopeng Sun, Zheng Fu, Philippe Ciais, Xiaoming Feng, Jing Li, Bojie Fu

Received: 11 October 2022 | Revised: 23 January 2023 | Accepted: 24 February 2023

DOI: 10.1111/gcb.16657

Global Change Biology WILEY

RESEARCH ARTICLE

Compound droughts slow down the greening of the Earth

Xianfeng Liu[1,2] | Gaopeng Sun[1] | Zheng Fu[2] | Philippe Ciais[2] | Xiaoming Feng[3] | Jing Li[1] | Bojie Fu[1,3]

[1]School of Geography and Tourism, Shaanxi Normal University, Xi'an, China

[2]Laboratoire des Sciences du Climat et de l'Environnement, CEA-CNRS-UVSQ, Gif-sur-Yvette, France

[3]State Key Laboratory of Urban and Regional Ecology, Research Center for Eco-Environmental Sciences, Chinese Academy of Sciences, Beijing, China

Correspondence
Xianfeng Liu, School of Geography and Tourism, Shaanxi Normal University, Xi'an, China.
Email: xianfeng.liu@lsce.ipsl.fr

Zheng Fu, Laboratoire des Sciences du Climat et de l'Environnement, CEA-CNRS-UVSQ, Gif-sur Yvette, France.
Email: zheng.fu@lsce.ipsl.fr

Bojie Fu, State Key Laboratory of Urban and Regional Ecology, Research Center for Eco-Environmental Sciences, Chinese Academy of Sciences, Beijing 100085, China.
Email: bfu@rcees.ac.cn

Funding information
National Natural Science Foundation of China, Grant/Award Number: 41991230 and 42171095; The Fundamental Research Funds for the Central Universities, Grant/Award Number: GK202201008; The Open Foundation of the State Key Laboratory of Urban and Regional Ecology of China, Grant/Award Number: SKLURE2022-2-1; The Social Science Foundation of Shaanxi Province, Grant/Award Number: 2020D039

Abstract

Vegetation response to soil and atmospheric drought has raised extensively controversy, however, the relative contributions of soil drought, atmospheric drought, and their compound droughts on global vegetation growth remain unclear. Combining the changes in soil moisture (SM), vapor pressure deficit (VPD), and vegetation growth (normalized difference vegetation index [NDVI]) during 1982–2015, here we evaluated the trends of these three drought types and quantified their impacts on global NDVI. We found that global VPD has increased 0.22 ± 0.05 kPa·decade^{-1} during 1982–2015, and this trend was doubled after 1996 (0.32 ± 0.16 kPa·decade^{-1}) than before 1996 (0.16 ± 0.15 kPa·decade^{-1}). Regions with large increase in VPD trend generally accompanied with decreasing trend in SM, leading to a widespread increasing trend in compound droughts across 37.62% land areas. We further found compound droughts dominated the vegetation browning since late 1990s, contributing to a declined NDVI of 64.56%. Earth system models agree with the dominant role of compound droughts on vegetation growth, but their negative magnitudes are considerably underestimated, with half of the observed results (34.48%). Our results provided the evidence of compound droughts-induced global vegetation browning, highlighting the importance of correctly simulating the ecosystem-scale response to the under-appreciated exposure to compound droughts as it will increase with climate change.

KEYWORDS
atmospheric drought, climate change, compound droughts, soil drought, soil moisture, vapor pressure deficit, vegetation browning, vegetation greening

1 | INTRODUCTION

Drought poses large risks to ecosystem services and agricultural production because of their devastating impacts on the environment, economy, and society (Zhang, Keenan & Zhou, 2021). Generally, drought classied into four types including meteorological drought, soil drought, hydrological drought, and social–economic drought (Wilhite & Pulwarty, 2017), which are strongly-correlated with sustained precipitation deficit but various elements of hydrosphere response to drought in different degrees (AghaKouchak et al., 2015). The combination of interacting physical processes across several related droughts is referred to as the compound droughts (AghaKouchak et al., 2020; Li, Li, Chen, Xiang, et al., 2021), leading to a significant impact on ecosystem and multiple social–economic sectors than any single drought (Ciais et al., 2005; Lloret et al., 2012; Su et al., 2021; Williams et al., 2010). The most occurrence of

Xianfeng Liu and Gaopeng Sun contributes equally to the work.

compound droughts is the coincidence of atmospheric drought (high vapor pressure deficit [VPD]) and soil drought (low soil moisture [SM]) (Zhang, Gentine, et al., 2022; Zhou et al., 2021), exacerbating substantial impacts on vegetation greenness and productivity (Liu, Feng, et al., 2020; Lloret et al., 2012; Piao et al., 2014; Sulman et al., 2016; Williams et al., 2010). Earth system models showed that the compound droughts will increase under global warming until the end of this century (Meehl et al., 2014; Yuan et al., 2019; Zhou et al., 2021). However, our knowledge of compound droughts, for example, the intensity, duration, and hotspots of global compound, and its impacts on global vegetation greenness are still unclear. A global analysis of compound droughts between atmospheric and soil drought is therefore critical to improve our understanding of compound droughts-related impacts on terrestrial ecosystem carbon budget and achieve the sustainable development of global vegetation greenness and photosynthesis.

Global vegetation greenness has increased substantially since the 1980s (Chen et al., 2019; Zeng et al., 2017; Zhu et al., 2016), but these increased trends reduced or even reversed since late 1990s (Pan et al., 2018), primarily due to an increase in drought (Feng et al., 2021). Recent several studies indicate that high VPD, a proxy of atmospheric drought, is the dominant factor in controlling global vegetation growth and photosynthesis, because VPD has increased significantly along with the global warming trend and has a strong negative correlation with gross primary production (GPP) of terrestrial vegetation through regulating the leaf stomata conductance (Fu et al., 2022; Rawson et al., 1977; Yuan et al., 2019). Conversely, other studies argue that soil drought, proxy by SM, dominates global vegetation dynamic compared to a little stress by VPD by using solar-induced chlorophyll fluorescence (SIF) datasets (Liu, Gudmundsson, et al., 2020; Seneviratne et al., 2010). It should be noted that although low SM is known to affect plant physiology (Zhou et al., 2021), the positive feedback between atmosphere and SM significant exacerbates the adverse impacts on vegetation growth (Zhang, Gentine, et al., 2022; Zhou, Williams, et al., 2019; Zhou, Zhang, et al., 2019). Therefore, recent research has emphasized that both drivers of VPD and SM should be accounted for to explain the impact of compound droughts on vegetation growth in consideration of the strong coupling mechanism of land–atmosphere interaction. A recent study discussed the potential coupling impact of compound droughts by projected outputs (Zhou, Zhang, et al., 2019), however, the relative contributions of different droughts on vegetation growth are unknown.

To this end, we present a global analysis of changes in compound droughts and analyze the impact of compound droughts on global vegetation growth by using flux tower measurements, remotely sensed observations, and earth system model outputs. Specifically, we aim to address the following three questions: (1) what are the patterns of global compound droughts and their evolution during 1982–2015? (2) What are the contributions of compound droughts on global vegetation browning since 1990s? (3) Do earth system models capture the influence of compound droughts? The third question is important because future projections of the land carbon sink depend on how models capture the response of GPP to compound droughts.

2 | MATERIALS AND METHODS

2.1 | Eddy-covariance observations

We used half-hourly or hourly GPP, air temperature (*T*), VPD, soil water content (SWC), wind speed (WS), and incoming shortwave radiation (SR) from the FLUXNET2015 dataset of energy, water, and carbon fluxes and meteorological data, which has undergone a standardized set of quality control and gap filling (Pastorello et al., 2020) (Table S1). Data were already processed following a consistent and uniform processing pipeline, and all corrections were already applied to the available product (Fu et al., 2022). We used SWC, VPD, *T*, *P*, SR, atmospheric CO_2 concentration, and WS in the analysis. Annual variations of each variable are shown in Figure S1. GPP estimates from the night-time partitioning method were used for the analysis. Thirty-eight sites were selected to construct the model based on the following criteria: (1) the site should measure all above variables, (2) the effective continuous observational data of the site need no less than 10 years, and (3) the site need located in vegetated or adjacent to the global vegetation area based on the International Geosphere-Biosphere Programme (Table S2). Also, we selected another independent 15 sites with effective continuous observation time no less than 6 years to test the robustness of the model (Table S3).

2.2 | Normalized difference vegetation index data

The advanced very high-resolution radiometer normalized difference vegetation index (NDVI) data are acquired from the third-generation product data (GIMMS3g) of NOAA series of weather satellites. The GIMMS3g NDVI dataset is freely available on the NASA website (https://ecocast.arc.nasa.gov/data/pub/gimms/) and it has an approximately 8 km × 8 km spatial resolution and a 15-day temporal resolution. In this study, the 15-day data are integrated into annual values with the maximum value composite method and its pixel size is bi-linearly interpolated to 0.5° × 0.5° for the further analysis (Tucker et al., 2005; Yuan et al., 2019).

2.3 | Climate data

The monthly Climatic Research Unit (CRU) dataset releases global monthly meteorological data variables with 0.5° × 0.5° spatial resolution, which is based on the observation data derived from meteorological stations scattered across continents around the world except Antarctica (Harris et al., 2014). The gridded dataset can be acquired freely from the University of East Anglia website (https://sites.uea.ac.uk/cru/). In this study, we selected monthly mean air temperature, actual vapor pressure data, and monthly cumulative

precipitation from the latest version record, CRU TS v4.04 (Harris et al., 2020). The air temperature and actual vapor pressure data are used to estimate VPD across global vegetate areas.

We also used shortwave radiation and wind speed for global vegetation driving force analysis during 1982 to 2015 from ERA5, the fifth-generation ECMWF reanalysis for the global climate and weather for the past four to seven decades. We interpolated the spatial resolution to 0.5°×0.5° by using bi-linearly interpolated method. For global atmospheric CO_2 concentration data, we used monthly scale observation data at Mauna Loa observatory of NOAA (https://www.noaa.gov/) from 1982 to 2015.

2.4 | SM data

The Global Land Evaporation Amsterdam Model (GLEAM) is a set of algorithms for the estimation of terrestrial evaporation and root-zone SM from satellite data (www.GLEAM.eu). These output datasets can be utilized for global and regional large-scale hydrological applications, climate studies, and research about land–atmosphere feedbacks. In this study, we used global SM observation data of each month from 1982 to 2015, and interpolated the spatial resolution to 0.5°×0.5° by using bi-linearly interpolated method.

2.5 | Landcover data

GLASS-GLC (Global Land Cover) product is developed by using the Google Earth Engine platform, using the global GLASS CDR dataset from 1982 to 2015 as the data source, covering seven land cover categories including cultivated land, forest, grassland, shrub, tundra, bare land, and ice and snow (Liu, Gong, Wang, et al., 2020). In this study, we constrain global vegetated areas to the overlap regions of cropland, forest, grass land, shrubland, and tundra from 1982 to 2015, and the following analysis is all based on the spatial boundary of global vegetated areas (Figure S2).

2.6 | Earth system models

Following the observational analysis, the same analysis was carried out for the three earth system models participating in the Coupled Model Inter-comparison Project Phase 6 (CMIP6). We used three earth system models, namely MPI-ESM-1-2-HAM, MPI-ESM1-2-LR, and AWI-ESM-1-1-LR, that simultaneously simulated root-zone SM (rzwc), net shortwave surface radiation (rss), relative humidity (hur), near-surface wind speed (sfcWind), near-surface air temperature (Tas), sea level pressure (psl), and gross primary production (gpp). The daily or monthly historical simulation datasets during 1982–2014 were retrieved from https://esgf-node.llnl.gov. The daily rzwc is further resampled to monthly to be consistent with other variables in the analysis. The CO_2 concentration simulation data are obtained from MPI-ESM-1-2-HAM. The average values of these three earth system models were used for the results.

2.7 | Calculation of VPD

The VPD commonly estimates as the difference between the saturation vapor pressure (SVP) and actual vapor pressure (AVP) (Yuan et al., 2019). The empirical formula is as below:

$$\mathrm{VPD} = \mathrm{SVP} - \mathrm{AVP} \tag{1}$$

$$\mathrm{SVP} = 6.112 \times f_w \times e^{\frac{17.67T_a}{T_a+243.5}} \tag{2}$$

$$f_w = 1 + 7 \times 10^{-4} + 3.46 \times 10^{-6} P_{mst} \tag{3}$$

$$P_{mst} = P_{msl}\left(\frac{(T_a+273.16)}{(T_a+273.16)+0.0065\times Z}\right)^{5.625} \tag{4}$$

where Z refers to DEM, and T_a and AVP are land air temperature and actual vapor pressure of CRU dataset, respectively. The latitude dependence of the correlation between VPD and temperature is discussed in Supplementary Information.

2.8 | Compound drought identification

Atmospheric drought is defined as high VPD percentiles (VPD > 90th percentile of VPD over the entire study period) while soil drought is defined as low SM percentiles (SM < 10th percentile of SM over the entire study period) in this study. Compound droughts are thus identified when an atmospheric drought coincides with a soil drought for a given pixel during 1982–2015 (Figure S3).

2.9 | Identification of TP of NDVI trend

We used the piecewise linear regression method to determine the TP of NDVI during 1982–2015. The piecewise linear regression model has been widely used in vegetation dynamics and climate analyses because it can effectively detect a TP in long time-series data (Tomé & Miranda, 2004; Wang et al., 2010). The equation is as follows:

$$y = \begin{cases} \beta_0 + \beta_1 t + \varepsilon & t \le \alpha \\ \beta_0 + \beta_1 t + \beta_1 (t-\alpha) + \varepsilon, & t \le \alpha \end{cases} \tag{5}$$

where y is NDVI; t is the time; and α is the TP of the time series; β_0 is the intercept; β_1 and $\beta_1+\beta_2$ denote the magnitude of the trends before and after the TP, respectively; and ε is the residual random error. α is determined by least square error methods.

2.10 | Theil–Sen trend analysis

The advantage of the SEN trend analysis method is that it does not require samples to obey a certain distribution, and has a strong ability to avoid measurement errors or outliers (Sen, 1968).

$$\beta = \text{median}\left(\frac{x_j - x_i}{j - i}\right) \forall j > i \quad (6)$$

where β is the vegetation change trend. x_i and x_j are the values of the vegetation index at time i and j, when $\beta > 0$, it means that the vegetation cover is increasing, and when $\beta > 0$, it means that the vegetation cover is showing a decreasing trend.

Mann–Kendall is a nonparametric statistical test method used to judge the significance of trends, which does not require samples to follow a certain distribution and is also free from the interference of a few outliers. The statistical value Z obtained from the analysis represents the change trend of the data. The positive and negative values of Z correspond to the upward and downward trends, respectively. At the same time, if Z value is greater than 1.64, it means that the significance test with a confidence level of 95% has been passed ($p < .05$).

2.11 | Pearson correlation analysis

Pearson correlation coefficient is used to reflect the degree of linear correlation between two variables X and Y. The value of R is between −1 and 1, and the greater the absolute value is, the stronger the correlation is. The population correlation coefficient ρ is defined as the ratio of the covariance between two variables X and Y and the product of their standard deviations, as follows:

$$R = \frac{\sum_{i=1}^{n}(X_i - \overline{X})(Y_i - \overline{Y})}{\sqrt{\sum_{i=1}^{n}(X_i - \overline{X})}\sqrt{\sum_{i=1}^{n}(Y_i - \overline{Y})}} = \frac{1}{n-1}\sum_{i=1}^{n}\left(\frac{X_i - \overline{X}}{\sigma_X}\right)\left(\frac{Y_i - \overline{Y}}{\sigma_Y}\right) \quad (7)$$

where $\frac{X_i - \overline{X}}{\sigma_X}$, $\overline{X}$, and σ_X are the standard fraction, sample mean, and sample standard deviation of the sample X_i, respectively, and n is the sample size. The long-term trend of time-series data is removed by using the detrend fluctuation analysis method before correlation analysis. The t-test is used for significance test of Pearson correlation coefficient analysis.

2.12 | Quantifying the effect of predictors on vegetation growth

The random forest (RF) model was used to separate the impact of compound droughts on vegetation growth. We first constructed RF models for simulating annual NDVI (or GPP) at each pixel driven by SM, VPD, SM × VPD (C), air temperature (T), precipitation (P), shortwave radiation (SR), atmospheric CO_2 concentration (CO_2), and wind speed (WS). Before training the model, all the variables were normalized. Then, 5000 trees were used to avoid a few decision trees being sensitive to data changes, and could reduce certain noises that are easy to produce over-fitting. For training the model, we randomly choose 60% samples for training, 20% samples for validation, and 20% samples for test to build the model. Cross-validation method was used to select the best model. We then performed two simulations by using the well-validated RF model. We first run the model to simulate the annual NDVI with variable climate factors over time (experiment 1), and then run the model by fixing one climate factor in 1982 over time (experiment 2). The differences between the above two experiments could determine the influence of the fixed climate factor on vegetation growth. Details can be referred to Figure S4. To test the robustness of these results, we conduct the above analysis for both flux tower measurements and remote sensed observations, and achieve similar results (Figures S5 and S6). All above analysis is based on "the Random Forest" package in R platform (https://cran.r-project.org/web/packages/randomForest/).

3 | RESULTS

3.1 | Changes in global VPD and SM

Global mean annual VPD showed a significant increasing trend during 1982–2015, with an average rate of 0.22 ± 0.05 kPa·decade^{-1} ($p < .05$). The piecewise regression model indicated faster upward rate after year of 1996 (0.32 ± 0.16 kPa·decade^{-1}, $p < .05$) than that for before (0.16 ± 0.15 kPa·decade^{-1}, $p < .05$). Spatially, 72.92% (33.89% significant at $p < .05$, hereafter) and 27.08% (1.47%) regions of global vegetated areas displayed increasing and decreasing trends in VPD, respectively. The largest VPD trend mainly distributed in grasslands, savannas, croplands, and tropical rainforests in Africa and Brazil, with a rate more than 0.5 kPa·decade^{-1} ($p < .05$) and occupy approximately 18.01% of vegetated land (Figure 1a,b). Conversely, SM did not present an obvious trend during study period, and had a comparable proportion of increasing and decreasing trend regions, with 53.29% (10.51%) and 46.71% (8.53%), respectively (Figure 1c,d). The spatial differences for VPD and SM before and after 1996 also suggest a more prominent increasing trend of VPD after year of 1996 (Figure S7).

The global distribution of correlation coefficients between VPD and SM showed a prominent latitude heterogeneity, with high positive correlations in tropical regions and gradually decreased with the increase in latitude, especially in the Northern Hemisphere. Spatially, approximately 78.3% areas of global vegetated regions show a significant correlation at $p < .05$. Moreover, more than 90% areas present negative correlation between VPD and SM, and prominent negative correlation ($p < .05$) in South Asia, Amazon and Congo rainforest, and Sahel regions, suggesting regions with large increase in VPD trend generally accompanied with decrease trend in SM, contributing an increasing trend in concurrent of high VPD and low SM events during the studied period (Figure 1e,f).

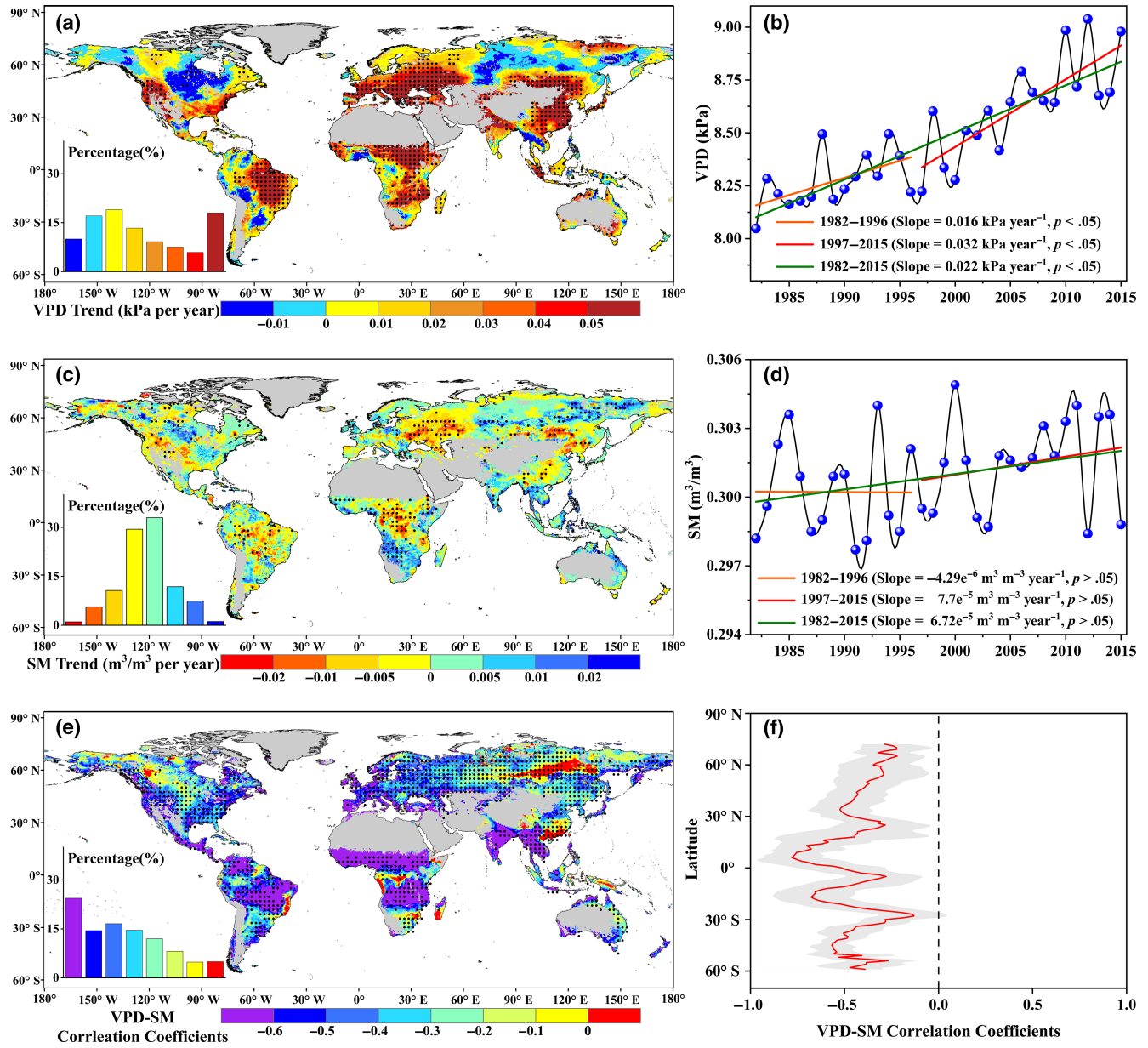

FIGURE 1 Spatiotemporal variations in trend of VPD (a) and SM (c), with their annual variation curve (b, d), respectively. Subfigure (e) is the spatial distribution of correlation coefficients between detrended SM and detrended VPD, and its latitude variation (f). The dots in (a, c, e) indicate significant at $p < .05$, and gray areas indicate non-vegetated regions. SM, soil moisture; VPD, vapor pressure deficit. [Colour figure can be viewed at wileyonlinelibrary.com]

3.2 | Changes in atmospheric drought, soil drought, and their compound droughts

The results of 15-year moving window to detect changes in soil drought, atmospheric drought, and concurrent drought (VPD > 90% and SM < 10%) show that 40.27% (22.8% significant at $p < .01$, hereafter) regions of global vegetated areas experience an increasing soil drought during study period, while 59.73% (39.26%) regions witness a decreasing trend of soil drought (Figure 2a). For VPD extreme, 62.97% (43.78%) regions of global vegetated areas show a prominent increasing trend in atmospheric drought, and 37.03% (21.32%) regions show a decreasing trend in atmospheric drought (Figure 2b). For compound droughts, our results show a significant increasing trend over 1982–2015, regions with increasing and decreasing trend are 54.93% and 45.07%, respectively, indicating strong coupling between soil drought and atmospheric drought (Figure 2c). Moreover, we find that more extreme drought shows more significant increase or decrease trends. Regions with significant increase in concurrent drought primarily concentrated in the Middle and Eastern Europe, the Middle and Northeastern China, the South American, the South Brazil, and Sahel regions.

We further binned SM and VPD into 10 percentile classes, and calculated the concurrent trend of SM and VPD in different SM-VPD intervals (Figure 2d). We found that high VPD (VPD > 60%) presents an increasing trend in all available SM bins, and it tends to reach maximum trend for compound extremes events. Moreover,

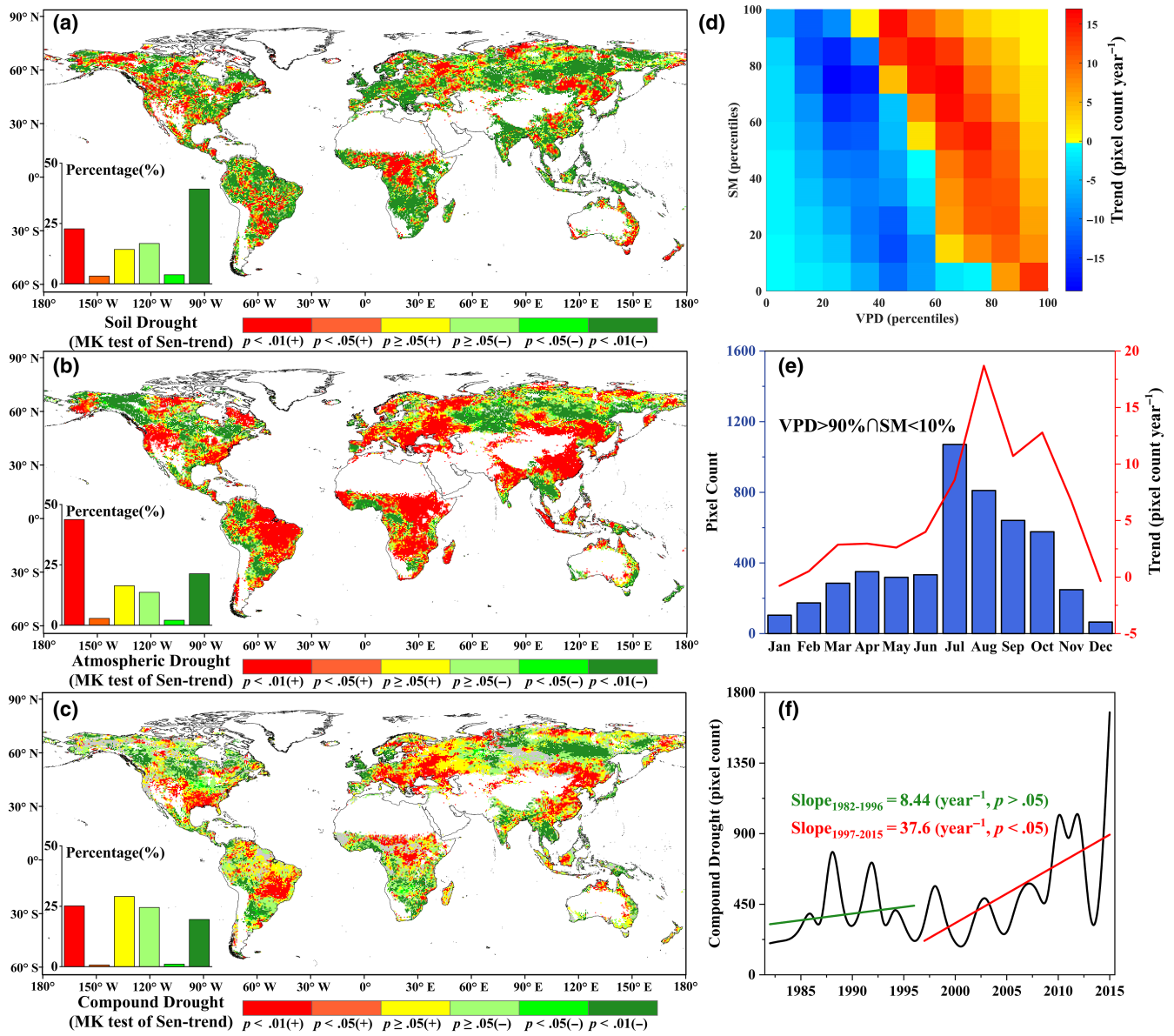

FIGURE 2 Spatial distributions of soil drought (a), atmospheric drought (b), and compound droughts (c) from 1982 to 2015. (d) Trend of coupling areas between SM and VPD for each percentile bin, (e) is the intra annual pattern of compound droughts during the study period, and (f) is the inter annual changes in global averaged compound droughts. SM, soil moisture; VPD, vapor pressure deficit. [Colour figure can be viewed at wileyonlinelibrary.com]

the TPs of VPD from decreasing to increasing trend gradually became lower when SM increased, which suggest that more humid conditions may more sensitive to occur compound droughts. Temporally, the intra-annual pattern of compound droughts shows an uni-modal distribution, with both pixels counts and their increasing trend reach to the top at July–August, indicating compound droughts tend to occur in warm season (Figure 2e). The inter-annual variability of compound droughts show an overall increasing trend globally during 1982–2015, but the increasing trends during 1997–2015 are particularly high, which is significantly larger than in 1982–1996 (Figure 2f). These results indicate widespread regions experience a significant increasing trend in compound droughts and atmospheric drought during study period and mainly concentrated in warm seasons.

3.3 | Responses of vegetation activities to climatic factors

Global NDVI showed a significant greening trend, with an average rate of 0.0008 year^{-1} ($p < .05$) during 1982–2015, however, the trend is significantly slower during 1997–2015 (0.0002 year^{-1}, $p > .05$) compared to 1982–1996 (0.0014 year^{-1}, $p < .05$). Spatially, more than 50.79% of global vegetated areas show negative trend during 1997–2015, which is spatial consistency with the area of increased compound droughts during the period (Figure 3).

To quantitatively evaluate the response of vegetation growth to climatic factors, a RF model was used to reconstruct NDVI based on SM, VPD, SM × VPD (*C*), air temperature (*T*), precipitation (*P*), shortwave radiation (SR), atmospheric CO_2 concentration (CO_2), and wind

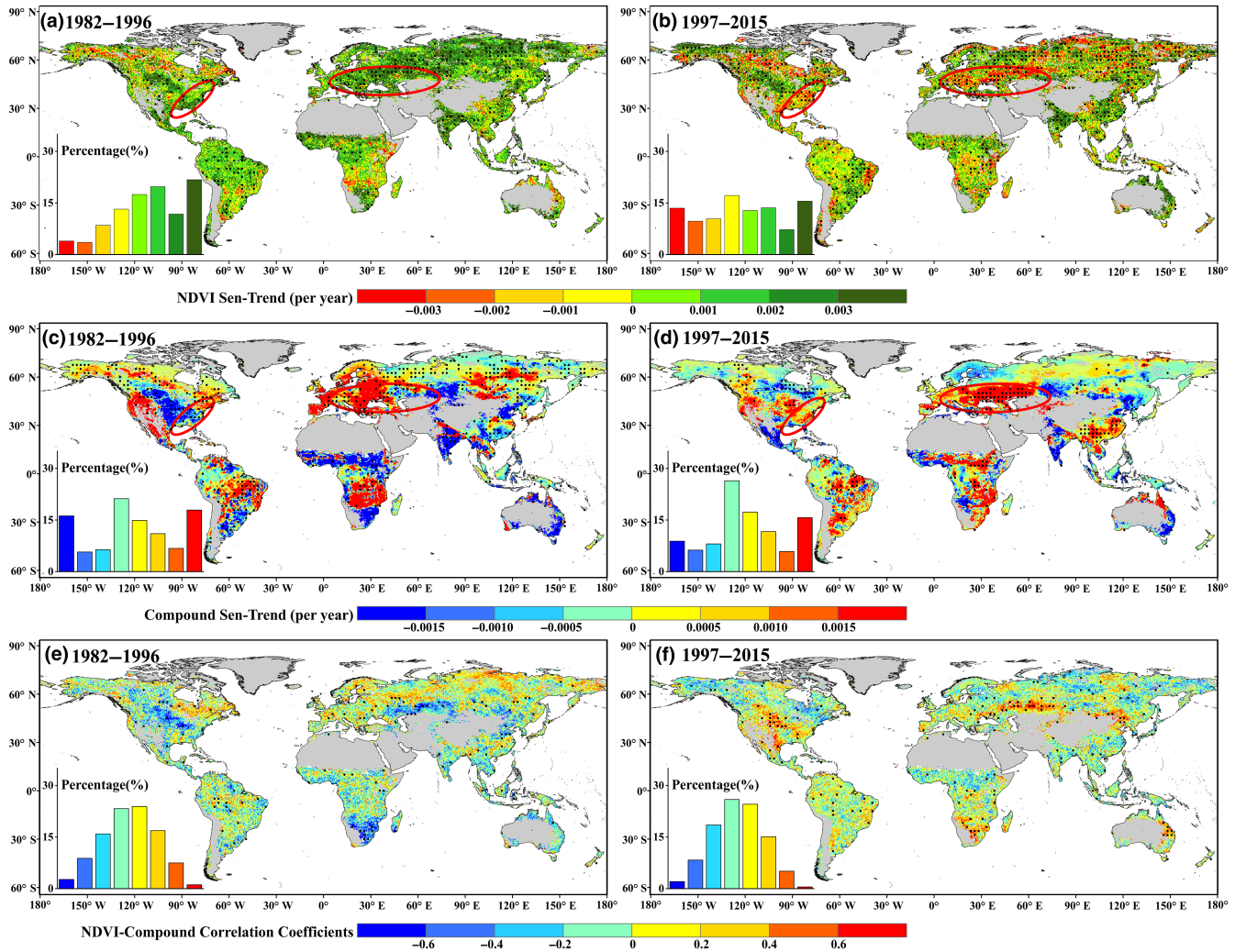

FIGURE 3 Spatial distribution of NDVI trends during 1982–1996 (a) and 1997–2015 (b), spatial distribution of compound droughts trends during 1982–1996 (c) and 1997–2015 (d), and the spatial distribution of correlation coefficients between NDVI and compound droughts during 1982–1996 (e) and 1997–2015 (f). The red circles in (a–d) highlighted the areas with significant increase in the trend of compound droughts. NDVI, normalized difference vegetation index. [Colour figure can be viewed at wileyonlinelibrary.com]

speed (WS). The predicted NDVI matches well with the observed NDVI, with R^2 of the test set is .946 during 1982–2015, and the highest correlation coefficients were observed across mid- and high latitude of the North Hemisphere (Figure 4; Figure S8). Then the model was applied to separate the impact of each climatic factor on NDVI. We first run the model to simulate the annual NDVI with variable climate factors over time (experiment 1), and then run the model by fixing one climate factor in 1982 over time (experiment 2). The differences between the above two experiments could determine the influence of the fixed climate factor on vegetation growth. The model experiments indicated that the increasing compound droughts significantly decreased NDVI (64.56%), following by VPD (28.08%) and wind speed (5.32%) during the period of global browning (1997–2015). Thus, compound droughts dominated the global browning. In contrast, CO_2 fertilization plays a significant role in stimulating vegetation growth (70.09%) during 1997–2015. However, the increased NDVI induced by CO_2 fertilization was nearly offset by the increased compound droughts, leading to a widespread browning of global vegetated areas (Figure 4c). We also calculated the sensitivity of vegetation anomaly to different independence variables, and found that compound droughts are the most sensitivity variable to drive vegetation decline (Figure 4d).

To test the robust of our results, we also repeated our analysis using global flux tower datasets from FLUXNET2015, and found that compound droughts posed large negative effect on NDVI/GPP among all variables (Figure 4e,f). Therefore, our findings indicate that the increased compound droughts dominant global vegetation browning during 1997–2015, which is in line with the substantial increase in compound droughts during 1997–2015 compared to 1982–1996.

3.4 | Earth system model simulations

To gain additional insights on the impact of compound droughts on vegetation growth, we analyze the response of vegetation

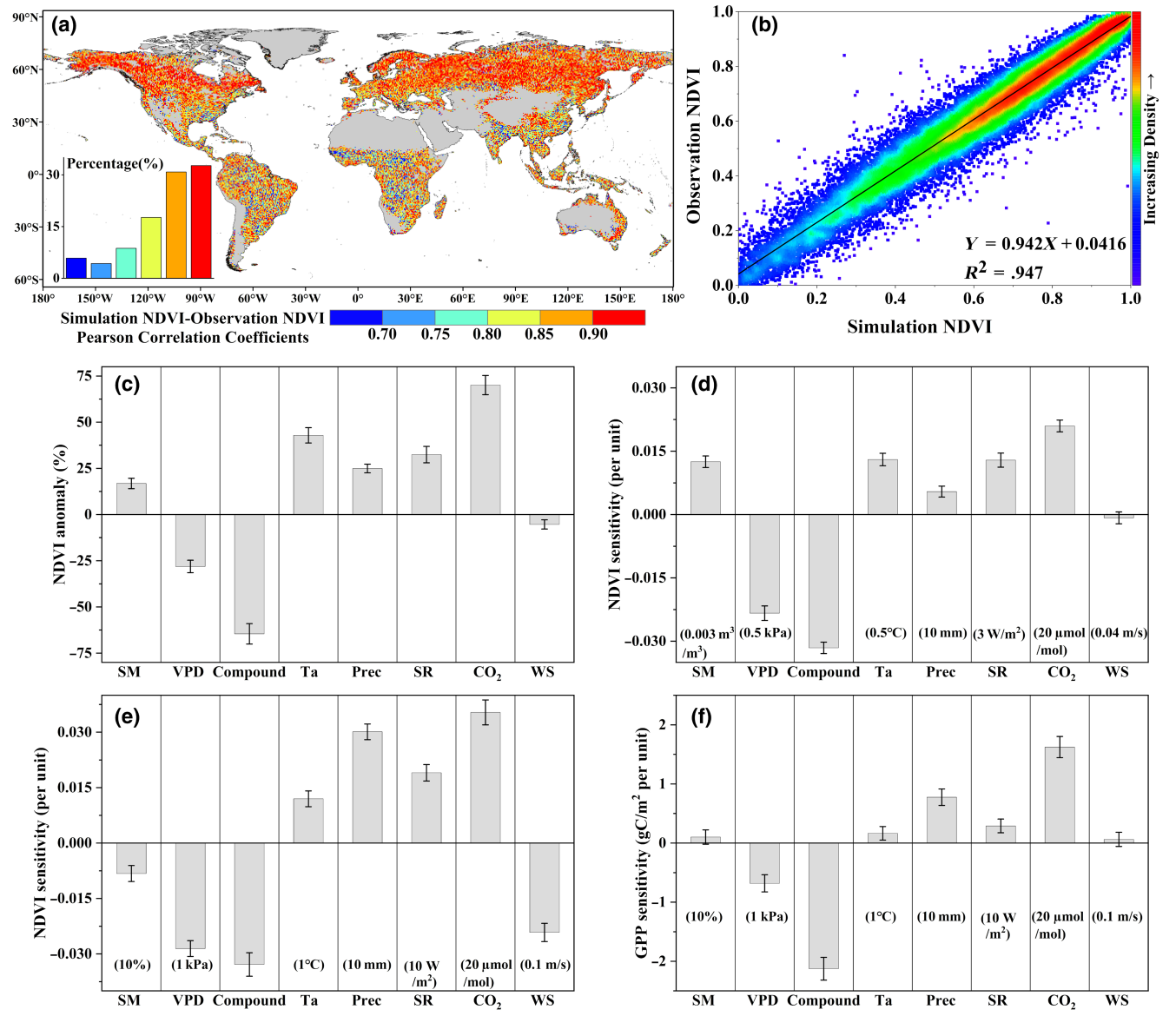

FIGURE 4 Random forest simulation of NDVI and the response of global NDVI to each predictor. (a) Spatial distribution of correlation coefficients between simulated NDVI and observed NDVI. (b) Scatter density plot of simulated NDVI and observed NDVI. (c) Percentage of NDVI anomaly induced by each predictor (%). (d) Sensitivity of NDVI to each predictor. The values in parentheses indicate the increments for each variable in sensitivity analysis. (e) and (f) are same as (d) but for NDVI and GPP from global flux tower datasets. GPP, gross primary production; NDVI, normalized difference vegetation index; SM, soil moisture; VPD, vapor pressure deficit. [Colour figure can be viewed at wileyonlinelibrary.com]

productivity to climate variables using the output from earth system models that simultaneously simulate all variables used in this work. Outputs from these models forced by observed climate fields and changing CO_2 concentration are analyzed for their predictions during the historical period 1982–2014. GPP is chosen as a dependent variable in RF model. The average values of these three earth system models were used for the analysis. The results share a similar pattern to the observed results, and also indicate a dominant role of compound drought impact on vegetation growth, providing two separate lines of evidence (i.e., both earth observing and model based) for compound droughts drives browning of the earth (Figure 5; Figures S9–S11). However, the ensemble model mean result shows that compound droughts could only decrease NDVI/GPP by 34.48%, nearly half of the observed results (Figure 5c), suggesting that the state-of-the-art model considerably underestimated the impact of compound droughts on global vegetation growth.

4 | DISCUSSION

4.1 | Substantial increase in coupling of soil and atmospheric droughts

Compound events refer to the combination of process (climate drivers and hazards) leading to a significant impact (Zscheischler et al., 2018), which have recently received more attention because

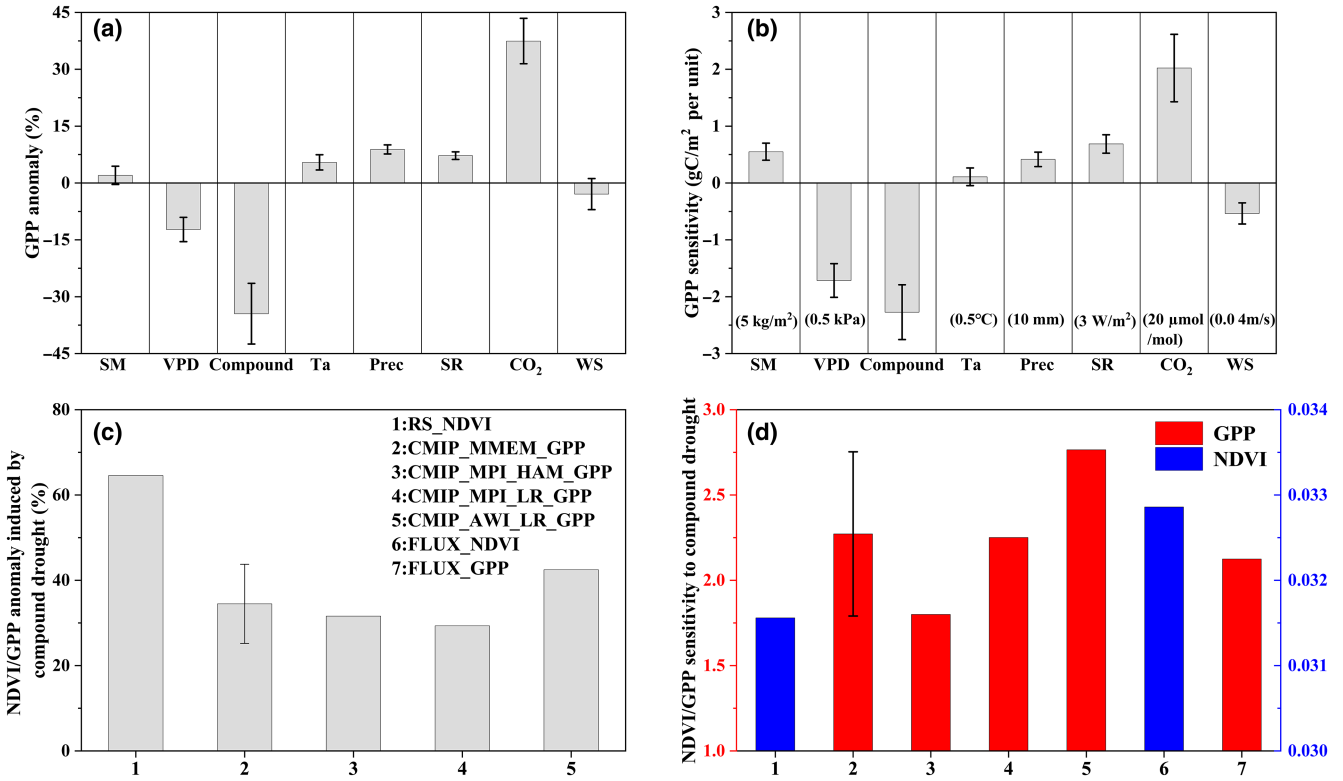

FIGURE 5 The response of GPP to each predictor in CMIP6 models. (a) Percentage of GPP anomaly induced by each predictor (%). (b) Sensitivity of GPP to each predictor. The value in parentheses indicates the increments for each variable in sensitivity analysis. (c) Compound drought-induced GPP or NDVI anomalies for satellite observations and three earth system models. (d) Sensitivities of GPP or NDVI to changes in compound droughts for satellite observations, three earth system models, and eddy-covariance measurements. The number in *x*-axis indicates different datasets. GPP, gross primary production; NDVI, normalized difference vegetation index; SM, soil moisture; VPD, vapor pressure deficit. [Colour figure can be viewed at wileyonlinelibrary.com]

of their devastating and large-scale impact on natural ecosystem, food system, human health, and economic stability (AghaKouchak et al., 2020; Frank et al., 2015; Lesk et al., 2021; Raymond et al., 2020; Zscheischler & Seneviratne, 2017). Most exist studies focus on the interactions between different hazards, including drought, heat waves, wildfires, and floods, and their significant impacts which occurs simultaneously. For example, Mazdiyasni and AghaKouchak (2015) indicate a substantial increase in concurrent droughts and heatwaves across most parts of the United States. Lesk et al. (2021) reported a stronger impact of climate warming on global crop yields when consider temperature–moisture coupling. Our results indicate a substantial increase in compound droughts of soil and atmosphere in many regions of the world, both in dryland and humid regions (Figure 3). The inherence of compound droughts is the propagation of drought across different hydrological process. For example, when precipitation decreases, atmospheric drought occurs first, followed by agricultural drought that measured by SM (Liu et al., 2016). The increase in compound droughts indicates that the propagation rate from atmospheric drought to soil drought has increased during recent decades, suggesting an acceleration of global hydrological cycle through positive feedback under global warming. That is, increased VPD increases the water demand of atmospheric drought, and further accelerates the loss of SM; in turn, decreased SM reduced evapotranspiration, accompanying with higher temperature and associated VPD, due to decreased latent cooling effect. In addition, traditional atmospheric drought or soil drought are long lasting and usually occur in all seasons or cross season, however, our results indicate that compound droughts of atmospheric and soil mainly occur in warm seasons and the drought period is generally shorter than the traditional single drought. Therefore, knowledge of the intensity, duration, and frequency of compound droughts is the presupposition for future compound drought prediction and adaption strategies under a changing climate.

4.2 | Dominant role of compound droughts in global vegetation browning

Over the past three decades, many studies have documented a greening trend of the earth during 1982–2015 (Chen et al., 2019; Zeng et al., 2017; Zhu et al., 2016). However, a recent study provides an interesting finding that an increasing global vegetation browning since late 1990s and attributed this phenomenon to drought (Pan et al., 2018). The outstanding issue has raised heated debate, for example, one study documents that the increased VPD significant reduces global vegetation growth since late 1990s (Yuan et al., 2019),

whereas the other study shows that low SM is the dominant driver of dryness stress on ecosystem production across more than 70% of vegetated land areas based on satellite observations of SIF (Liu, Gudmundsson, et al., 2020). Our results quantitatively demonstrate that the compound droughts of soil and atmospheric rather than a single type drought is the dominant factor to reduce NDVI since the late 1990s, for example, an increase in compound droughts across Middle and Eastern Europe and east America spatially coincides with a decrease in NDVI (Figure 3a–d). Although our results confirmed the negative role of VPD on global vegetation growth, but the negative effect was further amplified by the coupling of low SM and high VPD. Compared with a single factor, the increased demand of atmospheric water will further aggravate the loss of SM, thereby forming a positive feedback effect, making the impact of compound higher than two single factors. Specifically, as carbon starvation and hydraulic failure are the two main constrains on vegetation growth. When water stress occurs, the leaf stomatal conductance declines in order to reduce water consumption, accompanied by a decrease in CO_2 absorption through leaf stomach. These coupling processes of water stress and carbon reduce associated with extreme low SM and high VPD will pose considerable negative effect on vegetation growth and these trends will further intensify under global warming (Huang et al., 2016; Jiao et al., 2021; Lian et al., 2021). In addition, CMIP5 models show that the frequency and intensity of compound droughts of soil and atmospheric is projected to increase in the 21st century (Zhou, Zhang, et al., 2019), which will greatly undermine the vegetation greening trend and further induce vegetation mortality and reduced terrestrial carbon uptake.

We noted that there is an increased trend in compound droughts over regions such as south-eastern China and Sahel (Figure 3a–d), where show a persist greening trend after year of 1997. This is because the fact that these regions have been a substantial increase in afforestation and productive croplands over the past decades (Chen et al., 2019). In addition, we also noted that NDVI may suffer a saturation issue in densely forest (Atkinson et al., 2011), although NDVI is widely used in previous studies to detect vegetation growth in response to climate extremes and rising atmospheric CO_2 (Jong et al., 2013; Yang et al., 2023; Yuan et al., 2019; Zhang, Gentine, et al., 2022).

4.3 | Implications of compound droughts induced vegetation browning

The predominant role of compound droughts in causing the vegetation browning has important implications for understanding the ecosystem functions in response to climate change. Because climate change likely results in an increased frequency and intensity of drought (AghaKouchak et al., 2020; Wu et al., 2022), future changes in compound droughts may cause substantial reduction in carbon uptake by impacting the vegetation activities. In addition, compound droughts could increase the risk of vegetation mortality, resulting in the decrease in biodiversity and accelerating the degradation of ecosystem. Meanwhile, vegetation browning will also offset the cooling effects of global greening through land–atmospheric feedback (Zeng et al., 2017), which could further exacerbate the drought conditions, leading to larger carbon loss globally. To better simulate land carbon sink under changing climate, it is urgent for global models to realistically consider the impacts of compound droughts on terrestrial ecosystems.

Rising temperatures have also increased the occurrence, severity, and duration of heat waves and droughts, which in turn have increased the risk of wildfires (Raymond et al., 2020). However, most of current studies primarily focused compound event on the coupling of two related climate extremes or drivers, for example, drought and heatwaves (Lesk et al., 2021). Knowledge regarding the combination of more than two extremes or drivers is still in its infancy, particularly the nexus of drought, heatwaves, wildfire, and global carbon cycle is still an open question. Therefore, our findings highlight the need to improve our understanding of the interrelated climate extremes. Specifically, we need a systematic evaluation of compound events, including definitions and types, research frameworks, impact assessments, and future trends prediction. This will help to better predict the impacts of compound events on the capacity of continents to act as a carbon sink in the future.

5 | CONCLUSIONS

We analyzed the changes in atmospheric drought, soil drought, and compound droughts, and quantified the response of global vegetation dynamic to different droughts. The results show a significant increasing trend in global averaged VPD during 1982–2015, and the upward rate doubled after 1996 than before 1996. Regions with large increase in VPD trend generally accompanied with decrease trend in SM, leading to a widespread increasing trend in compound droughts across the most land area fraction. RF model experiments suggest a divergent response of vegetation dynamics to different climate drivers during study period, and our results showed a dominant role of compound droughts in causing vegetation browning since late 1990s. Earth system models also suggest the dominant role of compound droughts on vegetation growth, but the negative magnitude of GPP anomaly is considerably underestimated.

AUTHOR CONTRIBUTIONS

Xianfeng Liu designed the research. Gaopeng Sun performed the analysis, and Xianfeng Liu wrote the paper with the inputs from all co-authors. Zheng Fu, Philippe Ciais, Xiaoming Feng, Jing Li, and Bojie Fu contributed to the interpretation of the results and discussions.

ACKNOWLEDGMENTS

This study was sponsored by the National Science Foundation (Nos. 41991230, 42171095), the Social Science Foundation of Shaanxi Province (2020D039), the Fundamental Research Funds for the Central Universities (GK202201008), and the Open Foundation of

the State Key Laboratory of Urban and Regional Ecology of China (SKLURE2022-2-1).

CONFLICT OF INTEREST STATEMENT

The authors declare no competing interests.

DATA AVAILABILITY STATEMENT

The authors thank the Climatic Research Unit of university of East Anglia (https://www.uea.ac.uk), the Climate Change Service Program (https://climate.copernicus.eu/), the Global Land Evaporation Amsterdam Model (https://www.gleam.eu/), National Tibetan Plateau/Third Pole Environment Data Center of China (https://data.tpdc.ac.cn), National Oceanic and Atmospheric Administration (https://www.noaa.gov/), Annual dynamics of global land cover from 1982 to 2015 (https://doi.pangaea.de/10.1594/PANGAEA.913496), and FLUXNET Network (https://fluxnet.org/), for providing global datasets of CRU, ERA5, GLEAM-SM, GIMMS3g-NDVI, Atmospheric Mean CO_2 Concentrations, GLASS-GLC and FLUXNET2015. This work used global eddy-covariance data acquired and shared by the FLUXNET community, including these networks: AmeriFlux, AfriFlux, AsiaFlux, CarboAfrica, CarboEuropeIP, CarboItaly, CarboMont, ChinaFlux, Fluxnet Canada, GreenGrass, ICOS, KoFlux, LBA, NECC, OzFlux-TERN, TCOS-Siberia, and USCCC.

CODE AVAILABILITY STATEMENT

The code used in this analysis is available upon request from the corresponding authors.

ORCID

Xianfeng Liu https://orcid.org/0000-0001-6576-0711
Gaopeng Sun https://orcid.org/0000-0001-9810-901X
Zheng Fu https://orcid.org/0000-0001-7627-8824
Philippe Ciais https://orcid.org/0000-0001-8560-4943
Xiaoming Feng https://orcid.org/0000-0002-6761-0829
Jing Li https://orcid.org/0000-0001-7185-145X
Bojie Fu https://orcid.org/0000-0002-9920-9802

REFERENCES

AghaKouchak, A., Chiang, F., Huning, L. S., Love, C. A., Mallakpour, I., Mazdiyasni, O., Moftakhari, H., Papalexiou, S. M., Ragno, E., & Sadegh, M. (2020). Climate extremes and compound hazards in a warming world. *Annual Review of Earth and Planetary Sciences*, *48*, 519–548. https://doi.org/10.1146/annurev-earth-071719-055228

AghaKouchak, A., Farahmand, A., Melton, F. S., Teixeira, J., Anderson, M. C., Wardlow, B. D., & Hain, C. R. (2015). Remote sensing of drought: Progress, challenges and opportunities. *Reviews of Geophysics*, *53*(2), 452–480. https://doi.org/10.1002/2014RG000456

Atkinson, P. M., Dash, J., & Jeganathan, C. (2011). Amazon vegetation greenness as measured by satellite sensors over the last decade. *Geophysical Research Letters*, *38*, L19105. https://doi.org/10.1029/2011GL049118

Chen, C., Park, T., Wang, X., Piao, S., Xu, B., Chaturvedi, R. K., Fuchs, R., Brovkin, V., Ciais, P., Fensholt, R., Tømmervik, H., Bala, G., Zhu, Z., Nemani, R. R., & Myneni, R. B. (2019). China and India lead in greening of the world through land-use management. *Nature Sustainability*, *2*(2), 122–129. https://doi.org/10.1038/s41893-019-0220-7

Ciais, P., Reichstein, M., Viovy, N., Granier, A., Ogée, J., Allard, V., Aubinet, M., Buchmann, N., Bernhofer, C., Carrara, A., Chevallier, F., De Noblet, N., Friend, A. D., Friedlingstein, P., Grünwald, T., Heinesch, B., Keronen, P., Knohl, A., Krinner, G., … Valentini, R. (2005). Europe-wide reduction in primary productivity caused by the heat and drought in 2003. *Nature*, *437*(7058), 529–533. https://doi.org/10.1038/nature03972

Feng, X., Fu, B., Zhang, Y., Pan, N., Zeng, Z., Tian, H., Lyu, Y., Chen, Y., Ciais, P., Wang, Y., Zhang, L., Cheng, L., Maestre, F. T., Fernández-Martínez, M., Sardans, J., & Penuelas, J. (2021). Recent leveling off of vegetation greenness and primary production reveals the increasing soil water limitations on the greening Earth. *Science Bulletin*, *66*(14), 1462–1471. https://doi.org/10.1016/j.scib.2021.02.023

Frank, D., Reichstein, M., Bahn, M., Thonicke, K., Frank, D., Mahecha, M. D., Smith, P., van der Velde, M., Vicca, S., Babst, F., Beer, C., Buchmann, N., Canadell, J. G., Ciais, P., Cramer, W., Ibrom, A., Miglietta, F., Poulter, B., Rammig, A., … Zscheischler, J. (2015). Effects of climate extremes on the terrestrial carbon cycle: Concepts, processes and potential future impacts. *Global Change Biology*, *21*(8), 2861–2880. https://doi.org/10.1111/gcb.12916

Fu, Z., Ciais, P., Prentice, I. C., Gentine, P., Makowski, D., Bastos, A., Luo, X., Green, J. K., Stoy, P. C., Yang, H., & Hajima, T. (2022). Atmospheric dryness reduces photosynthesis along a large range of soil water deficits. *Nature Communications*, *13*, 989. https://doi.org/10.1038/s41467-022-28652-7

Harris, I., Osborn, T. J., Jones, P., & Lister, D. (2020). Version 4 of the CRU TS monthly high-resolution gridded multivariate climate dataset. *Scientific Data*, *7*(1), 1–18. https://doi.org/10.6084/m9.figshare.11980500

Harris, I. P. D. J., Jones, P. D., Osborn, T. J., & Lister, D. H. (2014). Updated high-resolution grids of monthly climatic observations–The CRU TS3. 10 Dataset. *International Journal of Climatology*, *34*(3), 623–642. https://doi.org/10.1002/joc.3711

Huang, J., Yu, H., Guan, X., Wang, G., & Guo, R. (2016). Accelerated dryland expansion under climate change. *Nature Climate Change*, *6*(2), 166–171. https://doi.org/10.1038/nclimate2837

Jiao, W., Wang, L., Smith, W. K., Chang, Q., Wang, H., & D'Odorico, P. (2021). Observed increasing water constraint on vegetation growth over the last three decades. *Nature Communications*, *12*(1), 1–9. https://doi.org/10.1038/s41467-021-24016-9

Jong, R. D., Schaepman, M. E., Furrer, R., Bruin, S. D., & Verburg, P. H. (2013). Spatial relationship between climatologies and changes in global vegetation activity. *Global Change Biology*, *19*(6), 1953–1964. https://doi.org/10.1111/gcb.12193

Lesk, C., Coffel, E., Winter, J., Ray, D., Zscheischler, J., Seneviratne, S. I., & Horton, R. (2021). Stronger temperature–moisture couplings exacerbate the impact of climate warming on global crop yields. *Nature Food*, *2*(9), 683–691. https://doi.org/10.1038/s43016-021-00341-6

Li, H., Li, Z., Chen, Y., Xiang, Y., Liu, Y., Kayumba, P. M., & Li, X. (2021). Drylands face potential threat of robust drought in the CMIP6 SSPs scenarios. *Environmental Research Letters*, *16*(11), 114004. https://doi.org/10.1088/1748-9326/ac2bce

Lian, X., Piao, S., Chen, A., Wang, K., Li, X., Buermann, W., Huntingford, C., Peñuelas, J., Xu, H., & Myneni, R. B. (2021). Seasonal biological carryover dominates northern vegetation growth. *Nature Communications*, *12*(1), 1–10. https://doi.org/10.1038/s41467-021-21223-2

Liu, X., Feng, X., Ciais, P., Fu, B., Hu, B., & Sun, Z. (2020). GRACE satellite-based drought index indicating increased impact of drought over major basins in China during 2002–2017. *Agricultural and Forest Meteorology*, *291*, 108057. https://doi.org/10.1016/j.agrformet.2020.108057

Liu, H., Gong, P., Wang, J., Clinton, N., Bai, Y., & Liang, S. (2020). Annual dynamics of global land cover and its long-term changes from 1982

to 2015. *Earth System Science Data*, *12*(2), 1217–1243. https://doi.org/10.5194/essd-12-1217-2020

Liu, L., Gudmundsson, L., Hauser, M., Qin, D., Li, S., & Seneviratne, S. I. (2020). Soil moisture dominates dryness stress on ecosystem production globally. *Nature Communications*, *11*(1), 4892. https://doi.org/10.1038/s41467-020-18631-1

Liu, X., Zhu, X., Pan, Y., Li, S., Liu, Y., & Ma, Y. (2016). Agricultural drought monitoring: Progress, challenges, and prospects. *Journal of Geographical Sciences*, *26*(6), 750–767. https://doi.org/10.1007/s11442-016-1297-9

Lloret, F., Escudero, A., Iriondo, J. M., Martínez-Vilalta, J., & Valladares, F. (2012). Extreme climatic events and vegetation: The role of stabilizing processes. *Global Change Biology*, *18*(3), 797–805. https://doi.org/10.1111/j.1365-2486.2011.02624.x

Mazdiyasni, O., & AghaKouchak, A. (2015). Substantial increase in concurrent droughts and heatwaves in the United States. *Proceedings of the National Academy of Sciences of the United States of America*, *112*(37), 11484–11489. https://doi.org/10.1073/pnas.1422945112

Meehl, G. A., Moss, R., Taylor, K. E., Eyring, V., Stouffer, R. J., Bony, S., & Stevens, B. (2014). Climate model intercomparisons: Preparing for the next phase. *EOS Transactions American Geophysical Union*, *95*(9), 77–78. https://doi.org/10.1002/2014EO090001

Pan, N., Feng, X., Fu, B., Wang, S., Ji, F., & Pan, S. (2018). Increasing global vegetation browning hidden in overall vegetation greening: Insights from time-varying trends. *Remote Sensing of Environment*, *214*, 59–72. https://doi.org/10.1016/j.rse.2018.05.018

Pastorello, G., Trotta, C., Canfora, E., Chu, H., Christianson, D., Cheah, Y. W., Poindexter, C., Chen, J., Elbashandy, A., Humphrey, M., Isaac, P., Polidori, D., Reichstein, M., Ribeca, A., van Ingen, C., Vuichard, N., Zhang, L., Amiro, B., Ammann, C., … Law, B. (2020). The FLUXNET2015 dataset and the ONEFlux processing pipeline for eddy covariance data. *Scientific Data*, *7*(1), 1–27. https://doi.org/10.1038/s41597-020-0534-3

Piao, S., Nan, H., Huntingford, C., Ciais, P., Friedlingstein, P., Sitch, S., Peng, S., Ahlström, A., Canadell, J. G., Cong, N., Levis, S., Levy, P. E., Liu, L., Lomas, M. R., Mao, J., Myneni, R. B., Peylin, P., Poulter, B., Shi, X., … Chen, A. (2014). Evidence for a weakening relationship between interannual temperature variability and northern vegetation activity. *Nature Communications*, *5*(1), 1–7. https://doi.org/10.1038/ncomms6018

Rawson, H. M., Begg, J. E., & Woodward, R. G. (1977). The effect of atmospheric humidity on photosynthesis, transpiration and water use efficiency of leaves of several plant species. *Planta*, *134*(1), 5–10. https://doi.org/10.1007/BF00390086

Raymond, C., Horton, R. M., Zscheischler, J., Martius, O., AghaKouchak, A., Balch, J., Balch, J., Bowen, S. G., Camargo, S. J., Hess, J., Kornhuber, K., Oppenheimer, M., Ruane, A. C., Wahl, T., & White, K. (2020). Understanding and managing connected extreme events. *Nature Climate Change*, *10*(7), 611–621. https://doi.org/10.1038/s41558-020-0790-4

Sen, P. K. (1968). Estimates of the regression coefficient based on Kendall's tau. *Journal of the American Statistical Association*, *63*(324), 1379–1389. https://doi.org/10.1080/01621459.1968.10480934

Seneviratne, S. I., Corti, T., Davin, E. L., Hirschi, M., Jaeger, E. B., Lehner, I., Orlowsky, B., & Teuling, A. J. (2010). Investigating soil moisture–climate interactions in a changing climate: A review. *Earth-Science Reviews*, *99*(3–4), 125–161. https://doi.org/10.1016/j.earscirev.2010.02.004

Su, S., Zhu, C., Li, X., & Wang, Q. (2021). Dynamic global warming impact assessment integrating temporal variables: Application to a residential building in China. *Environmental Impact Assessment Review*, *88*, 106568. https://doi.org/10.1016/j.eiar.2021.106568

Sulman, B. N., Roman, D. T., Yi, K., Wang, L., Phillips, R. P., & Novick, K. A. (2016). High atmospheric demand for water can limit forest carbon uptake and transpiration as severely as dry soil. *Geophysical Research Letters*, *43*(18), 9686–9695. https://doi.org/10.1002/2016GL069416

Tomé, A. R., & Miranda, P. M. A. (2004). Piecewise linear fitting and trend changing points of climate parameters. *Geophysical Research Letters*, *31*(2), L02207. https://doi.org/10.1029/2003GL019100

Tucker, C. J., Pinzon, J. E., Brown, M. E., Slayback, D. A., Pak, E. W., Mahoney, R., Vermote, E., & El Saleous, N. (2005). An extended AVHRR 8-km NDVI dataset compatible with MODIS and SPOT vegetation NDVI data. *International Journal of Remote Sensing*, *26*(20), 4485–4498. https://doi.org/10.1080/01431160500168686

Wang, X. H., Piao, S., Ciais, P., Li, J., Friedlingstein, P., Koven, C., & Chen, A. (2010). Spring temperature change and its implication in the change of vegetation growth in North America from 1982–2006. *Proceedings of the National Academy of Sciences of the United States of America*, *108*(4), 1240–1245. https://doi.org/10.1073/pnas.1014425108

Wilhite, D., & Pulwarty, R. S., (Eds.) (2017). *Drought and water crises: Integrating science, management, and policy*. CRC Press. https://doi.org/10.1201/9781420028386

Williams, A. P., Allen, C. D., Millar, C. I., Swetnam, T. W., Michaelsen, J., Still, C. J., & Leavitt, S. W. (2010). Forest responses to increasing aridity and warmth in the southwestern United States. *Proceedings of the National Academy of Sciences of the United States of America*, *107*(50), 21289–21294. https://doi.org/10.1073/pnas.0914211107

Wu, J., Feng, Y., Liang, L. L., He, X. Y., & Zeng, Z. Z. (2022). Assessing evapotranspiration observed from ECOSTRESS using flux measurements in agroecosystems. *Agricultural Water Management*, *269*, 107706. https://doi.org/10.1016/j.agwat.2022.107706

Yang, H., Munson, S. M., Huntingford, C., Carvalhais, N., Knapp, A. K., Li, X. Y., Peñuelas, J., Zscheischler, J., & Chen, A. P. (2023). The detection and attribution of extreme reductions in vegetation growth across the global land surface. *Global Change Biology*, 1–12. https://doi.org/10.1111/gcb.16595

Yuan, W., Zheng, Y., Piao, S., Ciais, P., Lombardozzi, D., Wang, Y., Ryu, Y., Chen, G., Dong, W., Hu, Z., Jain, A. K., Jiang, C., Kato, E., Li, S., Lienert, S., Liu, S., Nabel, J. E. M. S., Qin, Z., Quine, T., … Yang, S. (2019). Increased atmospheric vapor pressure deficit reduces global vegetation growth. *Science Advances*, *5*(8), eaax1396. https://doi.org/10.1126/sciadv.aax1396

Zeng, Z., Piao, S., Li, L. Z., Zhou, L., Ciais, P., Wang, T., Li, Y., Lian, X., Wood, E. F., Friedlingstein, P., Mao, J., Estes, L. D., Myneni, R.. B., Peng, S., Shi, X., Seneviratne, S. I., & Wang, Y. (2017). Climate mitigation from vegetation biophysical feedbacks during the past three decades. *Nature Climate Change*, *7*(6), 432–436. https://doi.org/10.1038/nclimate3299

Zhang, Y., Gentine, P., Luo, X. Z., Lian, X., Liu, Y. L., Zhou, S., Michalak, A. M., Sun, W., Fisher, J. B., Piao, S., & Keenan, T. F. (2022). Increasing sensitivity of dryland vegetation greenness to precipitation due to rising atmospheric CO_2. *Nature Communications*, *13*, 4975. https://doi.org/10.1038/s41467-022-32631-3

Zhang, Y., Keenan, T. F., & Zhou, S. (2021). Exacerbated drought impacts on global ecosystems due to structural overshoot. *Nature Ecology & Evolution*, *5*(11), 1490–1498. https://doi.org/10.1038/s41559-021-01551-8

Zhou, S., Williams, A. P., Berg, A. M., Cook, B. I., Zhang, Y., Hagemann, S., Lorenz, R., Seneviratne, S. I., & Gentine, P. (2019). Land–atmosphere feedbacks exacerbate concurrent soil drought and atmospheric aridity. *Proceedings of the National Academy of Sciences of the United States of America*, *116*(38), 18848–18853. https://doi.org/10.1073/pnas.1904955116

Zhou, S., Williams, A. P., Lintner, B. R., Berg, A. M., Zhang, Y., Keenan, T. F., Cook, B. I., Hagemann, S., Seneviratne, S. I., & Gentine, P. (2021). Soil moisture–atmosphere feedbacks mitigate declining water availability in drylands. *Nature Climate Change*, *11*(1), 38–44. https://doi.org/10.1038/s41558-020-00945-z

Zhou, S., Zhang, Y., Park Williams, A., & Gentine, P. (2019). Projected increases in intensity, frequency, and terrestrial carbon costs of compound drought and aridity events. *Science Advances*, *5*(1), eaau5740. https://doi.org/10.1126/sciadv.aau5740

Zhu, Z., Piao, S., Myneni, R. B., Huang, M., Zeng, Z., Canadell, J. G., Ciais, P., Sitch, S., Friedlingstein, P., Arneth, A., Cao, C., Cheng, L., Kato, E., Koven, C., Li, Y., Lian, X., Liu, Y., Liu, R., Mao, J., … Zeng, N. (2016). Greening of the earth and its drivers. *Nature Climate Change*, *6*(8), 791–795. https://doi.org/10.1038/nclimate3004

Zscheischler, J., & Seneviratne, S. I. (2017). Dependence of drivers affects risks associated with compound events. *Science Advances*, *3*(6), e1700263. https://doi.org/10.1126/sciadv.1700263

Zscheischler, J., Westra, S., Van Den Hurk, B. J., Seneviratne, S. I., Ward, P. J., Pitman, A., AghaKouchak, A., Bresch, D. N., Leonard, M., Wahl, T., & Zhang, X. (2018). Future climate risk from compound events. *Nature Climate Change*, *8*(6), 469–477. https://doi.org/10.1038/s41558-018-0156-3

SUPPORTING INFORMATION

Additional supporting information can be found online in the Supporting Information section at the end of this article.

How to cite this article: Liu, X., Sun, G., Fu, Z., Ciais, P., Feng, X., Li, J., & Fu, B. (2023). Compound droughts slow down the greening of the Earth. *Global Change Biology*, *29*, 3072–3084. https://doi.org/10.1111/gcb.16657